Experimental and numerical investigation of the effect of sample shapes on point load index

Hadi Haeri[*1], Vahab Sarfarazi[**2], Alireza Bagher Shemirani[3]
and Seyed Shahin Hosseini[4]

[1]*Young Researchers and Elite Club, Bafgh Branch, Islamic Azad University, Bafgh, Iran*
[2]*Department of Mining Engineering, Hamedan University of Technology, Hamedan, Iran*
[3]*Department of Civil Engineering, Sadra Institute of Higher Education, Tehran, Iran*
[4]*Department of Civil Engineering, Aria University of Sciences and Sustainability, Tehran, Iran*

Abstract. Tensile strength is considered key properties for characterizing rock material in engineering project. It is determined by direct and indirect methods. Point load test is a useful testing method to estimate the tensile strengths of rocks. In this paper, the effects of rock shape on the point load index of gypsum are investigated by PFC2D simulation. For PFC simulating, initially calibration of PFC was performed with respect to the Brazilian experimental data to ensure the conformity of the simulated numerical models response. In second step, nineteen models with different shape were prepared and tested under point load test. According to the obtained results, as the size of the models increases, the point load strength index increases. It is also found that the shape of particles has no major effect on its tensile strength. Our findings show that the dominant failure pattern for numerical models is breaking the model into two pieces. Also a criterion was rendered numerically for determination of tensile strength of gypsum. The proposed criteria were cross checked with the results of experimental point load test.

Keywords: point load test; failure pattern; breakage; PFC2D

1. Introduction

The point load test (PLT) is useful and cheap testing method to estimate the tensile and compressive strengths of rocks due to simplicity of sample preparation, its ease of testing and possible field application. Also, it's possible to performed point load test on irregular specimen. Protodyakonov and Voblikov (1957) have been the earliest to pursue systematically the testing of irregular specimens of rock, crushing them between two flat-surface platens. The paper by Broch and Franklin (1972), which popularized the point-load testing of drill cores, contains an extensive review of the topic. The ISRM commissions on testing methods (1972) issued recommended procedures for point-load testing. The revised recommended method for PL testing reflects repeated proposals to improve the method of calculating the PL strength index (Broch and Franklin

1972, Bieniawski 1975, Singh and Singh 1993, Chau and Wong 1996, Fener *et al.* 2005, Sonmez *et al.* 2004, 2006, Basu and Aydin 2006, Sönmez and Osman, 2008, Kahraman and Gunaydin 2009, Kayabal and Selcuk 2010, Ma 2010, Basu and Kamran 2010, Heidari *et al.* 2012, Singh 2012, Basu *et al.* 2013, Li *et al.* 2013, Haeri *et al.* 2014a, 2014b, 2015a, 2015b, 2015c, 2015d, 2015e, 2015f, Haeri 2015g, 2015h). Specimens can be of various shapes and be used to test both weak and strong rocks (ISRM 1985, Tsiambaos and Sabatakakis 2004, Society for Testing and Materials 2008, Kahraman and Gunaydin 2009, Heidari *et al.* 2012). There are different types of specimen geometries and testing procedures which can be used to evaluate compressive and tensile strengths under different loading conditions (Zhou *et al.* 2012, Ayatollahi and Alborzi 2013, Ramadoss and Nagamani 2013, Wei *et al.* 2015, Xu *et al.* 2015a, Kequan 2015, Lee 2015, Rajabi 2016, Mohammad 2016, Yaylac 2016). Determination of a correlation between uniaxial compressive strength/tensile strength and point load index (Is(50)) is one of the critical concerns in applying the point load test on various rock types. Numerous experimental test has shown that the conversion factors is different in igneous, metamorphic, and sedimentary rocks (Tsiambaos and Sabatakakis 2004, Kahraman *et al.* 2005, Fener *et al.* 2005, Kahraman and Gunaydin 2009, Heidari *et al.* 2012, Singh *et al.* 2012). The relationship between the Is(50) and Brazilian tensile strength is also often considered (Heidari *et al.* 2012). The objective of this paper is to determine the influences of specimen shape on the point-load index Is(50). Also a new criteria was rendered to determine tensile strength based on the Is(50).

2. Methods

2.1 Point load test methods
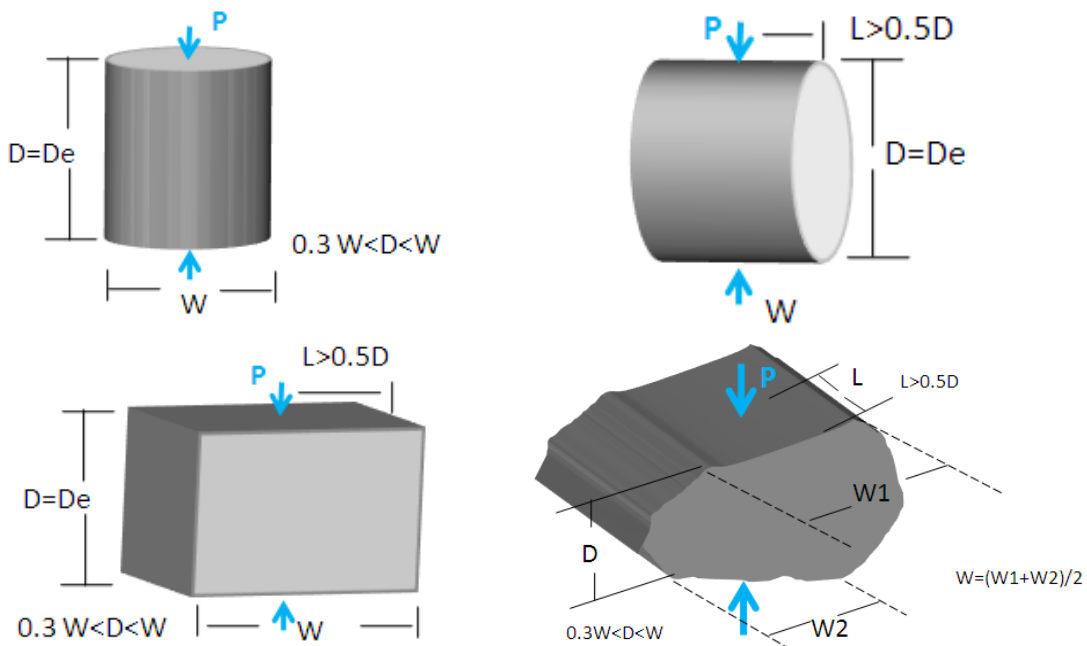

Fig. 1 Suggested methods for determining equivalent core diameter in irregular method

The methods suggested by ASTM (2008) is used for determining Is(50) with the following equation for the index

$$I_S(50) = F\left(\frac{P}{D_e^2}\right),\tag{1}$$

where P=peak load and De=equivalent core diameter for diametric and other states (De^2=4 A/π where A=WD, and W=the smallest specimen width perpendicular to the loading direction). If the sides of samples are not parallel, W is calculated as (W1+W 2)/2, as shown in Fig. 3, and D=distance between the platens at failure for axial point load testing, and =size correction factor, (D e/50)$^{0.45}$ (Fig. 1).

3. Numerical modelling

Particle flow code in two dimensions (PFC2D) was used for investigation of the effect of sample shape on both of the Is(50) and tensile strength.

3.1 Particle flow code

In simulation of rock by PFC2D, rock material is presented as an assembly of disks bonded together at their contact and confined by walls. There are two bonding models: a contact bonded model and a parallel bonded model. A contact bond approximates the physical behaviour of vanishingly small cement like substance lying between and joining the two bonded particles. The contact bond behaves as a parallel bond of radius zero. Thus, a contact bond does not have a radius or shear and normal stiffness's, as does a parallel bond, and cannot resist a bending moment; rather, it can only resist force acting at the contact point. The parallel bonds are assigned with specified tensile and shear strength which allows resistance to tension and shear to exist at the contacts until the force at the contact exceeds the strength of the bond. In order to generate a parallel bonded particle model for PFC2D, using the routines provided in (Cundall 1979), the following micro parameters should be defined: ball-to-ball contact modulus, stiffness ratio kn over ks, ball friction coefficient, contact normal bond strength, contact shear bond strength, ratio of standard deviation to mean of bond strength both in normal and shear direction, and mini mum Ball radius. Defining a parallel-bonded particle model requires three addition al micro parameters, which are: parallel-bond radius multiplier, parallel-bond modulus, and parallel-bond stiffness ratio.
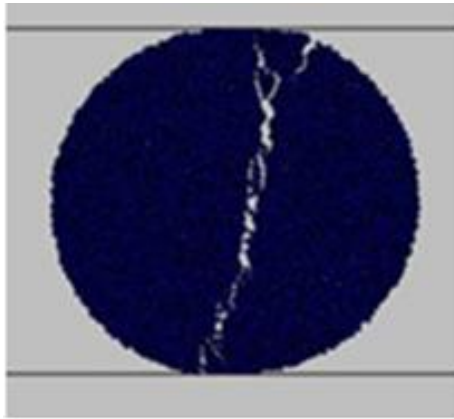
3.2 Preparing and calibrating the numerical model

Brazilian test was used to calibrate the tensile strength of model in PFC2D. Adopting the micro-properties listed in Table 1, with the standard calibration procedures (Potyondy and Cundall 2004), three calibrated PFC particle assembly was created. The diameter of the Brazilian disk considered in the numerical tests was 54 mm. The specimens were made of 5,615 particles with different clump particle distributed in it to gain the best results. The disk was crushed by the lateral walls moved toward each other with a low speed of 0.016 m/s. Fig. 2(a) and 2(b) illustrate the failure patterns in numerical and experimental tested samples, respectively. The failure planes experienced in numerical and laboratory tests are well matching.

Experimental measurements of tensile strength, 1 MPa, show good agreements with those of the numerical results, 1.1 MPa.

Table 1 Micro properties used to represent the model with tensile strength of 1.1 MPa

Property	Value	Property	Value
Type of particle	disc	Parallel bond radius muliplier	1.4
Densiy (kg/m^3)	2000	Youngs modulus of parallel bond (GPa)	40
Minimum radius (mm)	0.27	Parallel bond stifness ratio (pb_kn/pb_ks)	1.7
Size ratio	1.56	Particle friction coefficien	0.4
Porosity ratio	0.08	Parallel normal strength, mean (MPa)	5
Local damping coefficient	0.7	Parallel normal strength, std. dev (MPa)	2
Contact young modulus (GPa)	4	Parallel shear strength, mean (MPa)	5
Stiffness ratio (kn/ks)	1.7	Parallel shear strength, std. dev (MPa)	2
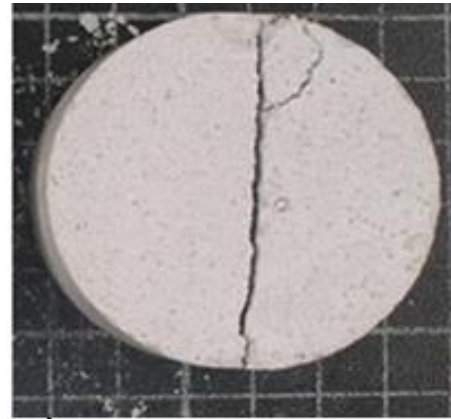
(a)   (b)

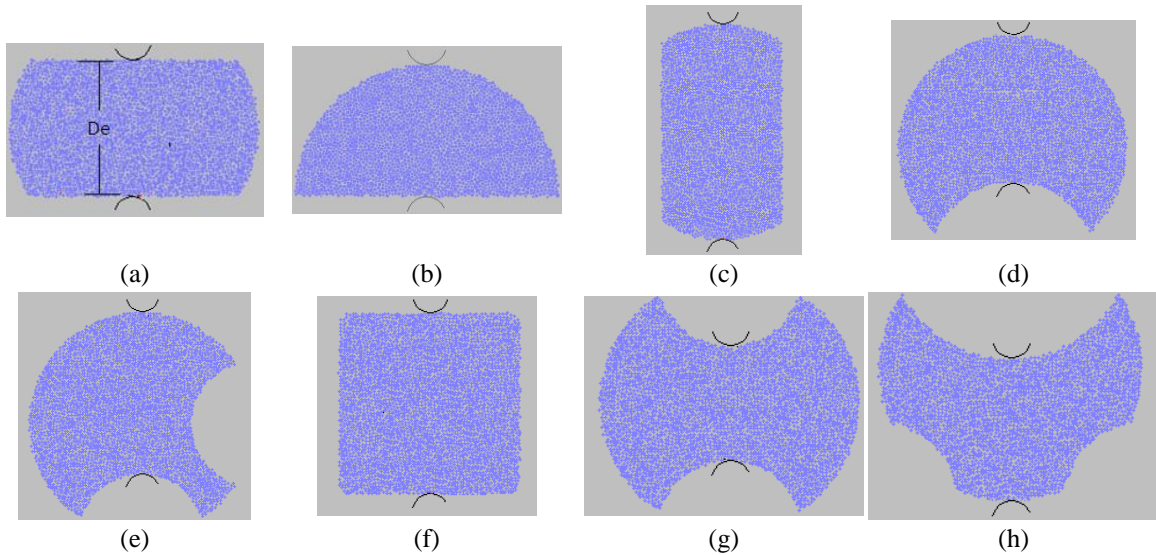Fig. 2 Failure pattern in (a) numerical model and (b) experimental samples

(a)   (b)   (c)   (d)

(e)   (f)   (g)   (h)

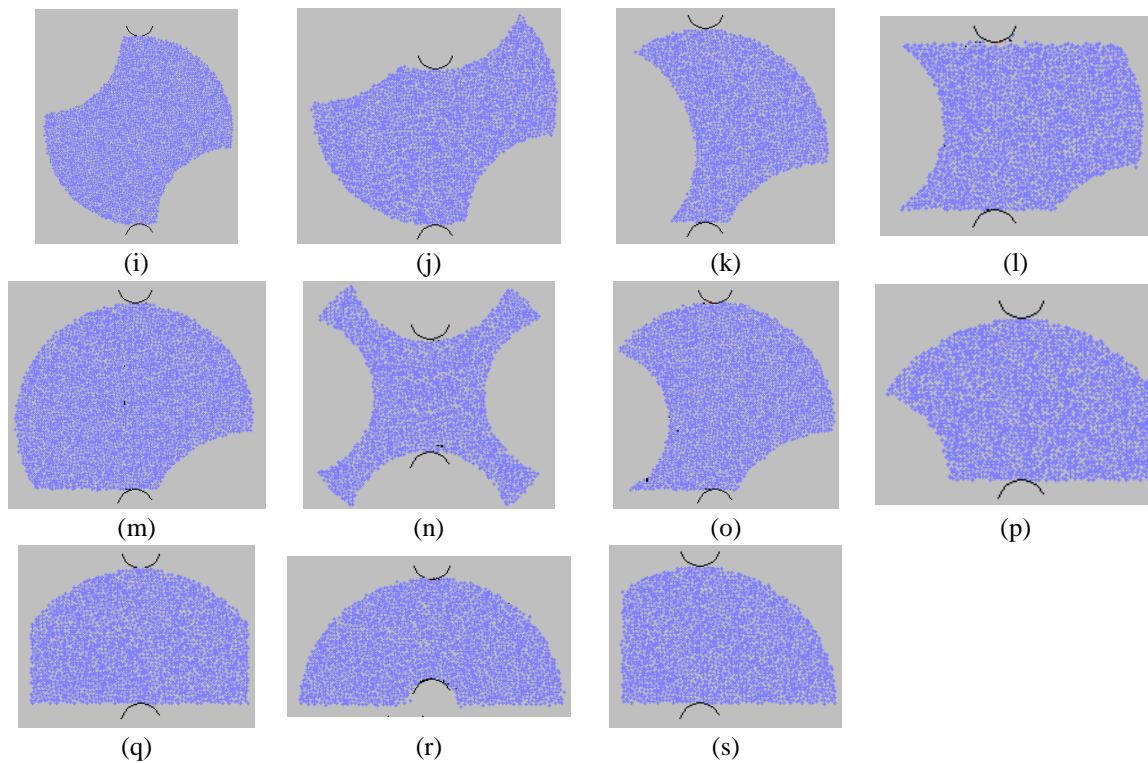Fig. 3 Various models with different shapes in PFC2D

Fig. 3 Continued

3.3 Numerical simulation of point load test

3.3.1 Preparing the model

After calibration of PFC2D, numerical simulation of point load test was simulated by creating a various model with different shape in the PFC2D (Fig. 3). Two loading walls were situated in top and bottom of the model. Upper wall moves in Y direction and lower wall moves in opposite side of Y direction with a low speed of 0.016 m/s.

Vertical Distance between two loading walls shown in Fig. 3(a), 3(b), 3(c), 3(d), 3(e), 3(f), 3(g), 3(h), 3(I), 3(j), 3(k), 3(l), 3(m), 3(n), 3(o), 3(p), 3(q), 3(r), and 3(s) were 25 mm, 27 mm, 54 mm, 44 mm, 40 mm, 35 mm, 24 mm, 29 mm, 54 mm, 33 mm, 35 mm, 40 mm, 48 mm, 24 mm, 38 mm, 30 mm, 30 mm, 25 mm and 30 mm.

3.3.2 Failure mechanism of sample with different shape

Fig. 4 shows progress of cracks in the models. Black line and red line represent tensile cracks and shear cracks, respectively. It's clear that tensile cracks are dominant mode of failure occurs in all models.

The failure of sample 1, 2, 4, 7, 14, 16, 17 and 19 (Fig. 4(a), 4(b), 4(d), 4(g), 4(n), 4(p), 4(q) and 4(s)) shows that tensile cracks initiates from wall-sample contacts and propagates nearly parallel to the loading direction till coalesces with each other. The failure of sample 5, 6, 12, 13 and 18 (Fig. 4(e), 4(f), 4(l), 4(m), 4(n) and 4(r)) shows that tensile major fractures initiates from wall-sample contacts and propagates nearly parallel to the loading direction till coalesces with

each other. Other tensile fractures initiates from wall-sample contact and propagate diagonally till coalesce with sample edge. The failure of sample 3, 8, 9, 10 and 11 (Fig. 4(c), 4(h), 4(i), 4(j), and 4(k)) shows that tensile cracks initiates from wall-sample lower contact and propagates diagonally for a short distance till coalesces with model edge. In this condition loading wall is in vicinity of sample edge, i.e., L<0.5 D, so non-ideal failure pattern occur in these samples. These results were not proper for analysis.
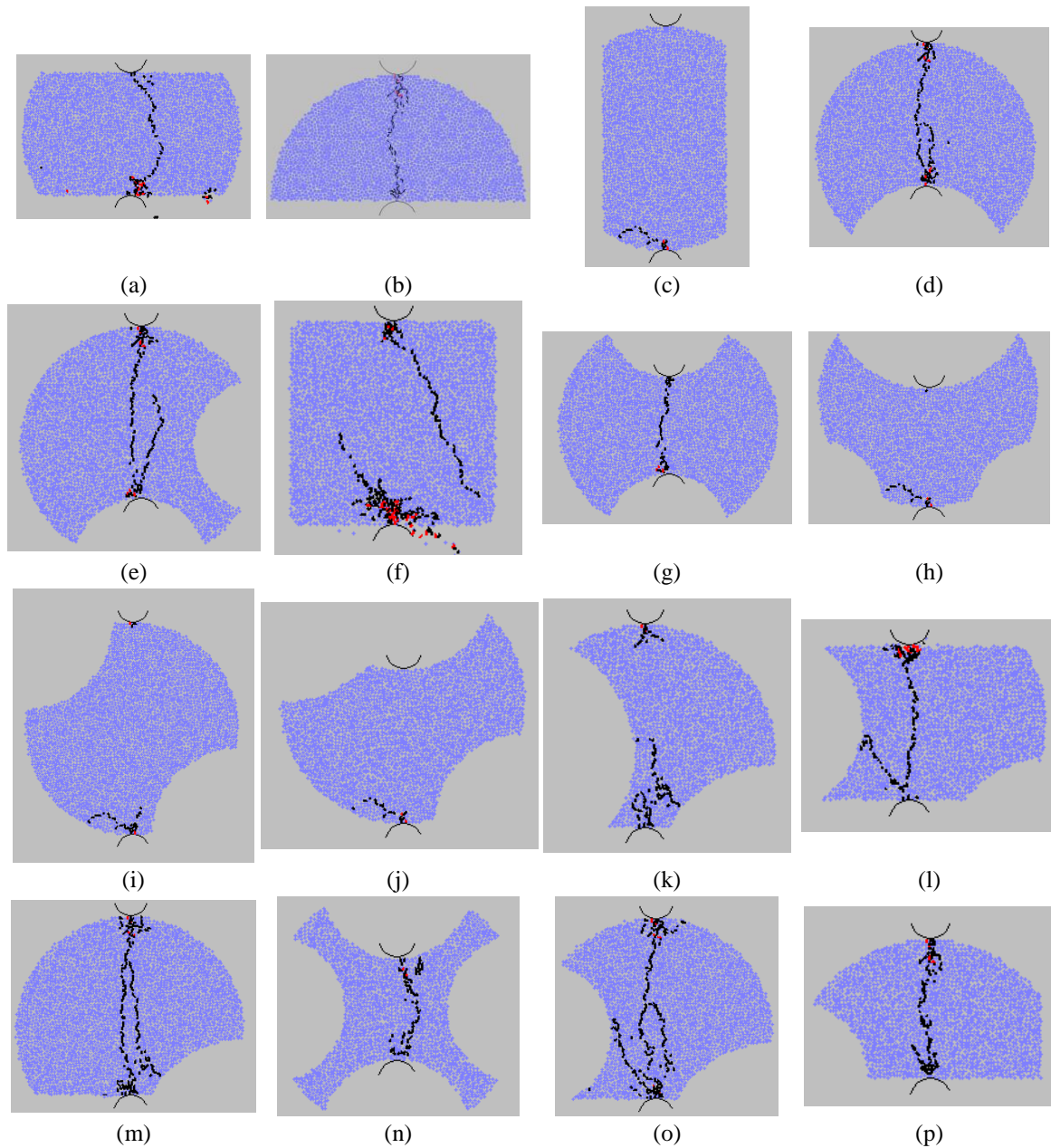

(a)   (b)   (c)   (d)

(e)   (f)   (g)   (h)

(i)   (j)   (k)   (l)

(m)   (n)   (o)   (p)

Fig. 4 Failure pattern in different models

(q)   (r)   (s)
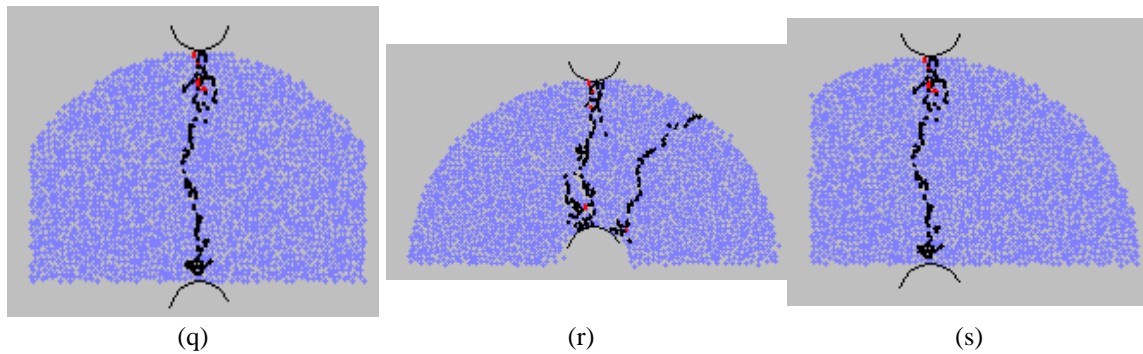
Fig. 4 Continued

Table 2 Is(50) in different Samples

Sample with different De (mm)	Is (50) (MPa)
24	0.407
24	0.405
25	0.415
25	0.416
27	0.431
29	0.452
30	0.468
30	0.468
30	0.468
35	0.518
40	0.578
40	0.578
44	0.650

3.4 Determination of Is$_{(50)}$ and relationship with tensile strength

The Is$_{(50)}$ for different samples, which have ideal failure pattern, was measured by equation 1 and listed in Table 2.

Fig. 5 shows variation of Is(50) with model diameter. Is(50) increases with increasing the model scale. The curve fitting equation on these data is

$$Is(50)=0.011*De+0.123 \tag{2}$$

De is model size between loading walls. Eq. (2) is useful for calculation of Is(50) based on model size. Fig. 5 shows normalized tensile strength with Is(50) versus model size. The normalized tensile strength with Is(50) decreases with increasing the model scale. The curve fitting equation on these data is

$$\sigma t/Is(50)=-0.05*De+3.887 \tag{3}$$

σt is tensile strength and can be calculated by Is(50) and model size, De.

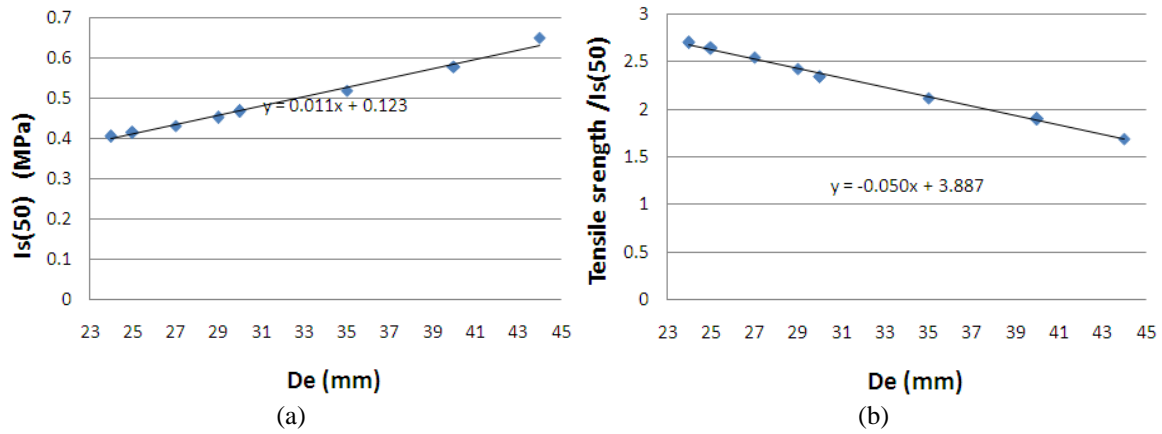(a)   (b)

Fig. 5 (a) variation of Is(50) related to equal core diameter (De) and (b) 16 variation of normalized tensile strength with Is(50) for different equal core diameter (De)
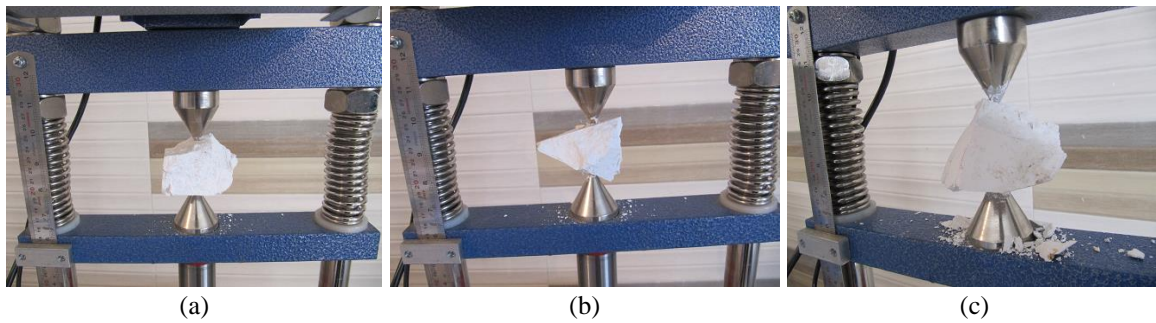

(a)   (b)   (c)

Fig. 6 Three different samples under point load test

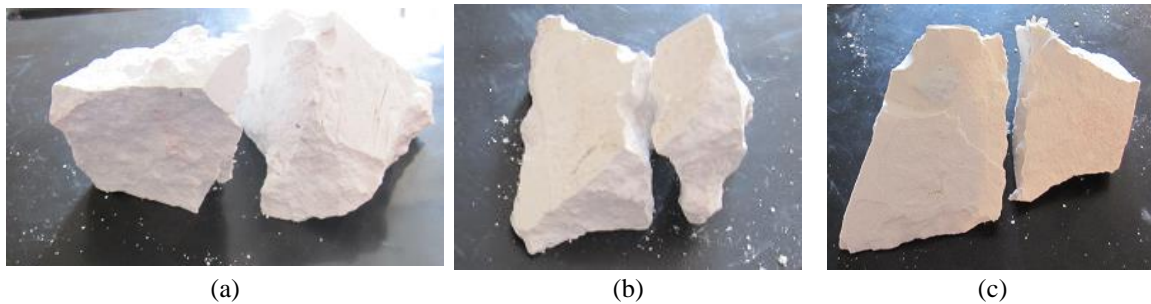(a)   (b)   (c)

Fig. 7 Failure pattern in different samples

Table 3 Is (50) calculated by Eq. (1) and tensile strength rendered by Eq. (3)

Sample number	Is(50)	Tensile strength (MPa)
1	0.56	1.2
2	0.45	1.15
3	0.52	1.25
Average		1.2

4. Experimental procedures

Three irregular specimens were prepared from the gypsum. A point load system of 100 kN load capacity with a deformation sensor (range=50 mm; resolution=0.01 mm) attached to the test frame was used (Fig. 6) in this investigation. The data acquisition system supplied by the manufacturer along with the instrument was used to continuously record the load and the corresponding displacement (i.e., depth of cone penetration) as a function of time throughout the tests.

A unique failure mode was observed in samples where the specimen failed in two pieces. The tensile cracks initiate from loading wedge and propagate within the model till coalescence with each other (Fig. 7). Inspection of failure surface shows that it was polished without pulverized material. These failure patterns are in a good accordance with those obtained by numerical simulation (Fig. 4).

The IS (50), calculated by Eq. (1), and tensile strength rendered by Eq. (3) were listed in Table 3. The results show that point load tensile strength was nearly equal to Brazilian tensile strength which is 1.1 MPa. A bit discrepancy between tensile strength results is due to differences between tensile force distributions on the failure surface.

5. Conclusions

Numerical point load test was performed to investigate the effect of sample shape on the point load index and tensile strength. Calibration of PFC was performed with respect to the Brazilian experimental data. Then, 19 models with different shape were built and tested under point load test. Concurrently, three gypsum samples were tested under point load condition. The results show that:

• When loading wall is in vicinity of sample edge, i.e., L<0.5 D, non-ideal failure pattern occurs in samples. The standard failure pattern occurs when L>0.5 D.

• Tensile cracks are dominant mode of failure occur in the numerical models. They initiate from wall-sample interfaces and propagates nearly parallel to the loading direction till coalesces with each other.

• Dominant failure pattern for numerical models is breaking the model into two pieces what occurs in experimental test.

• Is(50) increases with increasing the model scale.

• The shape of particles has no major effect on its tensile strength.

• The normalized tensile strength with Is(50) decreases with increasing the model scale.

• By inserting physical Is(50) in Eq. (3), tensile strength was determined which is nearly similar to Brazilian tensile strength.

• Comparison between numerical simulation and experimental test results shows that good accordance is established between them.

• Particle flow code is capable software for simulation of crack growth under point load test.

• This paper focus on the applicability of numerical simulation in prediction of point load index for gypsum block with different shapes. Whereas PFC was calibrated only for gypsum specimen, therefore the criterion rendered by numerical simulation is nearly capable to predict the tensile strength in this type of material. The authors attempt to do other new simulations on a wide range of crystalline rocks to present Is for crystalline rocks, too.

References

American Society for Testing and Materials (ASTM) (2008), *Standard Test Method for Determination of the Point Load Strength Index of Rock and Application to Rock Strength Classifications*, ASTM International, West Conshohocken, Pennsylvania, U.S.A.

Ayatollahi, M.R. and Alborzi, M.J. (2013), "Rock fracture toughness testing using SCB specimen", *Proceedings of the 13th International Conference on Fracture*, Beijing, China, June.

Bagi, K. (2012), *Fundamentals of the Discrete Element Method*, Lecture Notes, BME Faculty of Civil Engineering, Budapest, Hungary.

Basu, A. and Aydin, A. (2006), "Predicting uniaxial compressive strength by point load test: Significance of cone penetration", *Rock Mech. Rock Eng.*, **39**(5), 483-490.

Basu, A. and Kamran, M .(2010), "Point load test on schistose rocks and its applicability in predicting uniaxial compressive strength", *J. Rock Mech. Min. Sci.*, **47**(5), 823-828.

Basu, A., Mishra, D.A. and Roychowdhury, K. (2013), "Rock failure modes under uniaxial compression, Brazilian, and point load tests", *Bull. Eng. Geol. Environ.*, **72**(3-4), 457-475.

Bieniawski, Z.T. (1975), "The point-load test in geotechnical practice", *Eng. Geol.*, **9**(1), 1-11.

Broch, E. and Franklin, J.A. (1972), "The point-load strength test", *J. Rock Mech. Min. Sci. Geomech. Abstr.*, **9**(6), 669-676.

Celik, S.B. (2008), "Estimation of uniaxial compressive strength from point load strength, Schmidt hardness and P-wave velocity", *Bull. Eng. Geol. Environ.*, **67**(4), 491-498.

Chau, K.T. and Wong, R.H.C. (1996), "Uniaxial compressive strength and point load strength of rocks", *J. Rock Mech. Min. Sci. Geomech. Abstr.*, **33**(2), 183-188.

Fener, M., Kahraman, S., Bilgil, A. and Gunaydin, O. (2005), "A comparative evaluation of indirect methods to estimate the compressive strength of rocks", *Rock Mech. Rock Eng.*, **38**(4), 329-343.

Haeri, H. (2015g), "Propagation mechanism of neighboring vracks in rock-like cylindrical specimens under uniaxial compression", *J. Min. Sci.*, **51**(3), 487-496.

Haeri, H. (2015h), "Simulating the crack propagation mechanism of pre-cracked concrete specimens under shear loading conditions", *Strength Mater.*, **47**(4), 618-632.

Haeri, H., Khaloo, A. and Marji, M.F. (2015c), "Experimental and numerical simulation of the microcracks coalescence mechanism in rock-like materials", *Strength Mater.*, **47**(1), 740-754.

Haeri, H., Khaloo, A. and Marji, M.F. (2015d), "A coupled experimental and numerical simulation of rock slope joints behavior", *Arab. J. Geosci.*, **8**(9), 7297-7308.

Haeri, H., Khaloo, A. and Marji, M.F. (2015e), "Fracture analyses of different pre-holed concrete specimens under compression", *Acta Mech. Sinica*, **31**(6), 855-870.

Haeri, H., Khaloo, A. and Marji, M.F. (2015f), "Experimental and numerical analysis of Brazilian discs with multiple parallel cracks", *Arab. J. Geosci.*, **8**(8), 5897-5908.

Haeri, H., Marji, M.F. and Shahriar, K. (2015b), "Simulating the effect of disc erosion in TBM disc cutters by a semi-infinite DDM", *Arab. J. Geosci.*, **8**(6), 3915-3927.

Haeri, H., Shahriar, K., Marji, M.F. and Moarefvand, P. (2014a), "On the cracks coalescence mechanism and cracks propagation paths in rock-like specimens containing pre-existing random cracks under compression", *J. Central South U.*, **21**(6), 2404-2414.

Haeri, H., Shahriar, K., Marji, M.F. and Moarefvand, P. (2014b), "Investigating the fracturing process of rock-like Brazilian discs containing three parallel cracks under compressive line loading", *Strength Mater.*, **46**(3), 133-148.

Haeri, H., Shahriar, K., Marji, M.F. and Moarefvand, P. (2015b), "The HDD analysis of micro cracks initiation, propagation and coalescence in brittle substances", *Arab. J. Geosci.*, **8**(5), 2841-2852.

Heidari, M., Khanlari, G., Torabi Kaveh, M. and Kargarian, S. (2012), "Predicting the uniaxial compressive and tensile strengths of gypsum rock by point load testing", *Rock Mech. Rock Eng.*, **45**(2), 265-273.

International Society for Rock Mechanics (ISRM) (1985), "Suggested method for determining point load strength: ISRM common testing methods", *Rock Mech. Min. Sci. Geomech. Abstr.*, **22**(4), 112.

Kahraman, S. and Gunaydin, O. (2009), "The effect of rock classes on the relation between uniaxial compressive strength and point load index", *Bull. Eng. Geol. Environ.*, **68**(3), 345-353.

Kahraman, S., Gunaydin, O. and Fener, M. (2005), "The effect of porosity on the relation between uniaxial compressive strength and point load index", *J. Rock. Mech. Min. Sci.*, **42**(4), 584-589.

Kayabal, K. and Selçuk, L. (2010), "Nail penetration test for determining the uniaxial compressive strength of rock", *J. Rock. Mech. Min. Sci.*, **47**(2), 265-271.

Lee, S., Lee, S.H. and Chang, Y.S. (2015), "Evaluation of RPV according to alternative fracture toughness requirements", *Struct. Eng. Mech.*, **53**(6), 1271-1286.

Li, D. and Wong, L.N.Y. (2013), "Point load test on meta-sedimentary rocks and correlation to UCS and BTS", *Rock Mech. Rock Eng.*, **46**(4), 889-896.

Ma, G.W. and Wu, W. (2010), "Water saturation effects on sedimentary rocks", *Civil Eng. Res.*, **23**, 129-131.

Mosabepranah, M.A. and Eren, O. (2016), "Statistical flexural toughness modeling of ultra high performance concrete using response surface method", *Comput. Concrete*, **17**(4), 33-39.

Protodyakonov, M.M. and Voblikov, V.S. (1957), "Determining the strength of rock on samples of an irregular shape", *Ugol*, **32**(4).

Rajabi, M., Soltani, N. and Eshraghi, I. (2016), "Effects of temperature dependent material properties on mixed mode crack tip parameters of functionally graded materials", *Struct. Eng. Mech.*, **58**(2), 144-156.

Ramadoss, P. and Nagamani, K. (2013), "Stress-strain behavior and toughness of high-performance steel fiber reinforced concrete in compression", *Comput. Concrete*, **11**(2), 55-65.

Singh, T.N., Kainthola, A. and Venkatesh, A. (2012), "Correlation between point load index and uniaxial compressive strength for different rock types", *Rock Mech. Rock Eng.*, **45**(2), 259-264.

Singh, V.K. and Singh, D.P. (1993), "Correlation between point load index and compressive strength for quartzite rocks", *Geotch. Geol Eng.*, **11**(4), 269-272.

Sonmez, H. and Osman, B. (2008), "The limitations of point load index for predicting of strength of rock material and a new approach", *Proceedings of the 61st Geological Congress of Turkey*, **1**, 261-262.

Sonmez, H., Gokceoglu, C., Medley, E.W., Tuncay, E. and Nefeslioglu, H.A. (2006), "Estimating the uniaxial compressive strength of a volcanic bimrock", *J. Rock Mech. Min. Sci.*, **43**(4), 554-561.

Sonmez, H., Tuncay, E. and Gokceoglu, C. (2004), "Models to predict the uniaxial compressive strength and the modulus of elasticity for Ankara agglomerate", *J. Rock Mech. Min. Sci.*, **41**(5), 717-729.

Tsiambaos, G. and Sabatakakis, N. (2004), "Considerations on strength of intact sedimentary rocks", *Eng. Geol.*, **72**(3), 261-273.

Wei, M.D., Dai, F., Xu, N.W., Xu, Y. and Xia, K. (2015), "Three-dimensional numerical evaluation of the progressive fracture mechanism of cracked chevron notched semi-circular bend rock specimens", *Eng. Fract. Mech.*, **134**, 286-303.

Xu, N.W., Dai, F., Wei, M.D., Xu, Y. and Zhao, T. (2015a), "Numerical observation of three dimensional wing-cracking of cracked chevron notched Brazilian disc rock specimen subjected to mixed mode loading", *Rock Mech. Rock Eng.*, **49**(1), 79-96.

Yaylac, M. (2016), "The investigation crack problem through numerical analysis", *Struct. Eng. Mech.*, **57**(6), 1143-1156.

Yu, K. and Lu, Z. (2015), "Influence of softening curves on the residual fracture toughness of post-fire normal-strength concrete", *Comput. Concrete*, **15**(2), 102-111.

Zhou, Y.X., Xia, K., Li, X.B., Li, H.B., Ma, G.W., Zhao, J., Zhou, Z.L. and Dai, F. (2012), "Suggested methods for determining the dynamic strength parameters and mode-I fracture toughness of rock materials", *J. Rock. Mech. Min. Sci.*, **49**, 105-112.

CC